Tuning the Structure and Electronic Properties of B-N fused Dipyridylanthracene and Implications on the Self-Sensitized Reactivity with Singlet Oxygen

Kanglei Liu[a], Roger A. Lalancette[a], Frieder Jäkle[a,*]

[a] Department of Chemistry, Rutgers University-Newark, 73 Warren Street, Newark, NJ 07102, USA

* To whom correspondence should be addressed. Email: fjaekle@newark.rutgers.edu

Abstract. We demonstrate that the modification of anthracene with B←N Lewis pairs at their periphery serves as a highly effective tool to modify the electronic structure with important ramifications on the generation and reactivity towards singlet oxygen. A series of BN-fused dipyridylanthracene with Me groups in different positions of the pyridyl ring have been prepared via directed electrophilic borylation. The steric and electronic effects of the substituents on the structural features and electronic properties of the isomeric borane-functionalized products have been investigated in detail, aided by experimental tools and computational studies. We find that **BDPA-2Me** with Me groups adjacent to the pyridyl N has the longest B-N distance and shows overall less structural distortions, whereas **BDPA-5Me** with the Me group close to the anthracene backbone experiences severe distortions that are reflected in the buckling of the anthracene

framework and dislocation of the boron atoms from the planes of the phenyl rings they are attached to. The substitution pattern has also a dramatic effect on the self-sensitized reactivity of the acenes toward O_2 and the thermal release of singlet oxygen from the respective endoperoxides. Kinetic analyses reveal that **BDPA-2Me** very rapidly reacts with O_2, whereas **BDPA-5Me** is converted only very slowly to its endoperoxide. However, the latter serves as an effective singlet oxygen sensitizer as demonstrated in the preferential formation of the endoperoxide of dimethylanthracene in a competition experiment. These results demonstrate that even relatively small changes in the substitution of the pyridyl ring of BN-fused dipyridylanthracenes change the steric and electronic structure, resulting in dramatically different reactivity patterns. Our findings provide important guidelines for the design of highly effective sensitizers for singlet oxygen on one hand and the realization of materials that readily form endoperoxides in a self-sensitized manner and then thermally release singlet oxygen on demand on the other hand.

Introduction

The incorporation of heteroatoms presents a promising approach to judiciously alter the optical and electronic properties of organic π-conjugated materials.[1] By embedding electron-deficient boron atoms or replacing C-C for isoelectronic B-N units in particular, desirable properties such as acceptor character due to lower lying LUMO orbitals, red-shifted absorptions and emissions reaching into the near-IR, thermally activated delayed fluorescence (TADF), and enhanced charge carrier mobilities can be realized.[2] In a conceptually different approach the electronic structure of conjugated organic materials can also be modulated by B←N Lewis pair functionalization at their periphery. In this case, Lewis acid-base interactions result in the formation of tetra- rather than tricoordinate borane groups. Such an approach offers intriguing opportunities due to (i) the ensuing

planarization of the molecular skeleton that results in enhanced extension of π-conjugation and improved rigidity favoring radiative over non-radiative decay; (ii) the increased electron-deficient character due to lower LUMO levels upon attachment of the borane Lewis acid groups; (iii) the potential for stimuli-responsive "smart" materials and molecular switches enabled by the reversibility of the Lewis pair formation.[3]

Several methods are available for the attachment of B←N Lewis pairs including lithiation-borylation sequences, transition metal-catalyzed C-H borylation,[4] hydroboration of vinyl-functionalized derivatives,[5] or Lewis base-directed electrophilic borylation[6]. Taking advantage of these diverse synthetic routes, researchers have functionalized various N-heterocyclic-substituted conjugated organic materials with boron in an effort at developing new luminescent materials for OLEDs and imaging applications, electron transporting and acceptor materials for transistors and organic solar cells (OSCs), as well as photochromic and pH-switchable materials.[3d, 3e, 6b, 7]

We have recently embarked on an effort to explore the effects of the Lewis pair functionalization on larger π-conjugated scaffolds based on polycyclic aromatic hydrocarbons (PAHs). PAHs are attracting enormous research interest because of their desirable optical and electronic properties with applications ranging from organic electronics (OLEDs, OPVs, OFETs, singlet fission) to chemical sensors, catalysis and bioimaging.[8] They also serve important roles as models and building blocks for the bottom-up synthesis of larger conjugated carbon materials[1c, 9] and as components of supramolecular materials via Diels-Alder and photocyclization chemistries.[10] In addition, the ability of certain PAHs to reversibly form endoperoxides[11] can be exploited to deliver singlet oxygen for applications in photodynamic therapy,[12] in sensing,[13] lithography,[14] fluorescent anti-counterfeiting[15], and switches[16].

Efforts at the B←N Lewis pair functionalization of larger PAHs are only just emerging. Unique reactivity patterns have been uncovered,[17] intriguing molecular switching properties have been reported,[7e, 7f, 18] and circularly polarized luminescence (CPL) has been realized in the case of borylated helicenes.[19] We are pursuing the functionalization of PAHs by utilizing Lewis basic pyridyl[20] anchoring groups. In a first foray, we have recently demonstrated that the directed electrophilic borylation of dipyridylanthracene (**A**) results in selective borylation in the 1,5-positions[11c, 21] to give novel BN-fused polycyclic aromatic hydrocarbons (**B**, Figure 1).[22] The formation of the B←N Lewis pairs at the periphery of anthracene leads on one hand to planarization as the pyridyl groups adopt a more coplanar conformation with the anthracene core, but on the other hand induces significant steric strain that results in deformation (buckling) of the anthracene backbone. In addition, the BN units result in a polarization relative to the respective planarized all-carbon congener,[23] hence the LUMO is dramatically lowered and displays an enhanced quinoidal character relative to the all-carbon congener (**C**). Collectively, the planarization and polarization leads to an unusual change in color to deep red with a strong orange emission, as well as self-sensitized reactivity with O_2 to reversibly produce the corresponding endoperoxides.

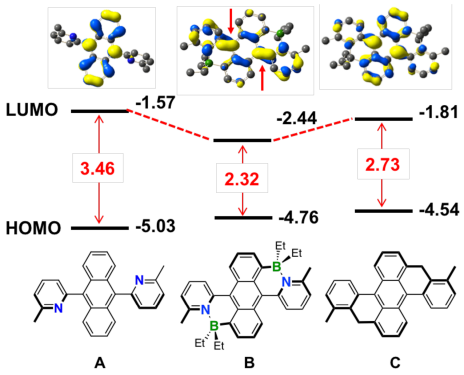

Figure 1. Structure, orbital energies (eV), and LUMO plot of borylated BN-anthracene **(B)** in comparison to the all-carbon analog (**C**) and the boron-free ligand (**A**).

As part of our continuing efforts to better understand the effects of borane functionalization on the structural features and electronic properties, in this work we have investigated four isomeric derivatives of BN-fused dipyridylanthracene with Me groups in different positions of the pyridyl ring. We find that the steric and electronic effects have a significant influence on the B←N bond strength, the extent of distortion, and the structural dynamics in this system. In addition, we demonstrate that different substituents dramatically affect the photophysical and electrochemical properties, as well as the self-sensitized reactivity of the acenes toward oxygen and the subsequent thermal release of singlet oxygen from the respective endoperoxides.

Result and Discussion

To examine the effects of different substituents on the B-N bond lengths, structural distortions and electronic properties of BN-fused dipyridylanthracene we first conducted DFT calculations on four isomeric derivatives with Me groups in different positions of the pyridyl rings, as well as the parent non-methylated species **BDPA** (Figure 2). We anticipated the methyl groups in derivatives **BDPA-3Me** and **BDPA-4Me** to have no significant steric influence, but to differ in terms of the electronic effects as 4-methylpyridine is expected to be a relatively stronger Lewis base. In contrast, the methyl groups in **BDPA-2Me** are expected to exert front strain that disfavors B←N Lewis pair formation, whereas steric strain in **BDPA-5Me** would be derived from interference of the methyl groups with the adjacent anthracene backbone protons in the 4 and 8-positions. We determined previously that the *cis*-isomer of **BDPA-2Me**, in which the pyridyl nitrogens point in the same direction and the boron atoms are dislocated from the anthracene backbone toward the same side, is significantly lower in energy than its *trans*-isomer.[22] Indeed, the same is true for all the other

compounds (Table S1) and the results of the calculations on the thermodynamically favored *cis*-isomers for **BDPA-3Me**, **BDPA-4Me** and **BDPA-5Me** are presented in the following.

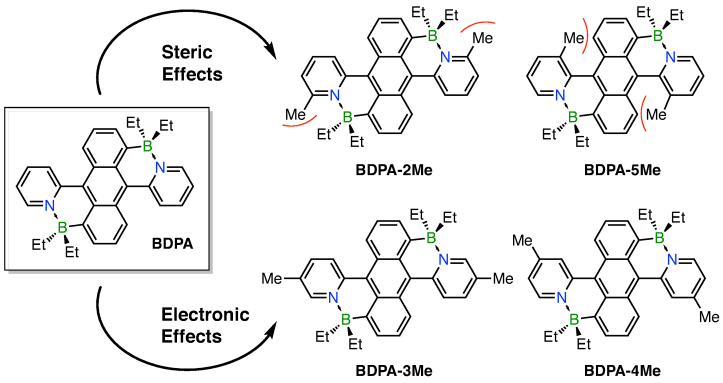

Figure 2. Structures of BN-anthracenes investigated by DFT methods.

Geometry optimization predicts the longest B-N distance for the previously reported derivative **BDPA-2Me** (1.690 Å) and the shortest for **BDPA-4Me** (1.640 Å) (Table 1). The relatively longer B-N distance for **BDPA-2Me** is consistent with steric interference between the Py-Me and BEt_2 groups, whereas the shorter B-N distance for **BDPA-4Me** highlights the enhanced Lewis basicity of 4-methylpyridine, though the differences between **BDPA-3Me**, **BDPA-4Me** and the non-methylated parent molecule are modest. An important observation is that the B-N distance for **BDPA-5Me** (1.655 Å) is significantly larger than that for **BDPA-3Me** (1.643 Å) (both have the Me group in *meta*-position), which suggests that remote steric effects also influence the strength of the B←N interactions. Indeed, by far the largest distortions to the anthracene backbone are found for **BDPA-5Me** with an interplanar angle between the terminal benzene rings of $\varepsilon = 25.6°$ (Figure 3). Another criterion to assess the steric strain is the dislocation of the boron atoms from the plane of the benzene rings that they are attached to. Again, the largest distortions are found for **BDPA-5Me** with Cent1-$C_{1,5}$-B angles of $\beta = 168.8°$ that significantly deviate from the ideal angle

of 180°. Our results suggest that in the case of **BDPA-5Me**, the close proximity of the Me substituents to the anthracene backbone results not only in strong "buckling" of the anthracene backbone, but also greater dislocation of the boron substituents and weaker B←N interactions. While the Me substituents in 2-position lead primarily to a lengthening of the B←N bonds, the molecule appears to be otherwise less distorted than **BDPA-3Me**, **BDPA-4Me**, or even the non-methylated derivative. This indicates that a lengthening of the B-N distance leads to a relaxation of the overall steric strain of the molecule.

Table 1. Comparison of computed geometric parameters of **BDPA** and its methyl-substituted derivatives (DFT, rb3lyp/6-31g(d))

Compound	B-N	B-$C_{1,5}$	$C_{9,10}$-C_{Py}	α [a]	β [b]	γ [c]	δ [d]	ε [e]	ϕ [f]
BDPA	1.642	1.619	1.471	105.3	171.2	165.4	18.4	21.3	36.2
BDPA-2Me	1.690	1.626	1.474	107.4	172.2	167.6	17.4	21.6	40.0
BDPA-3Me	1.643	1.618	1.471	105.5	171.0	165.8	18.1	20.7	35.4
BDPA-4Me	1.640	1.618	1.472	105.4	171.0	165.6	18.2	21.1	35.8
BDPA-5Me	1.655	1.618	1.474	105.7	168.8	167.3	20.9	25.6	42.2

[a] α = $C_{1,5}$-B-N angle; [b] β = Cent1-$C_{1,5}$-B; [c] γ = Cent2-$C_{9,10}$-C_{Py}; [d] δ = internal bending of central anthracene ring; [e] ε = $Ph_{An,out}$ // $Ph_{An,out}$, dihedral angle between outer anthracene rings; [f] ϕ = $Ph_{An,in}$ // Py, dihedral angle between inner anthracene ring and pendent pyridyl ring.

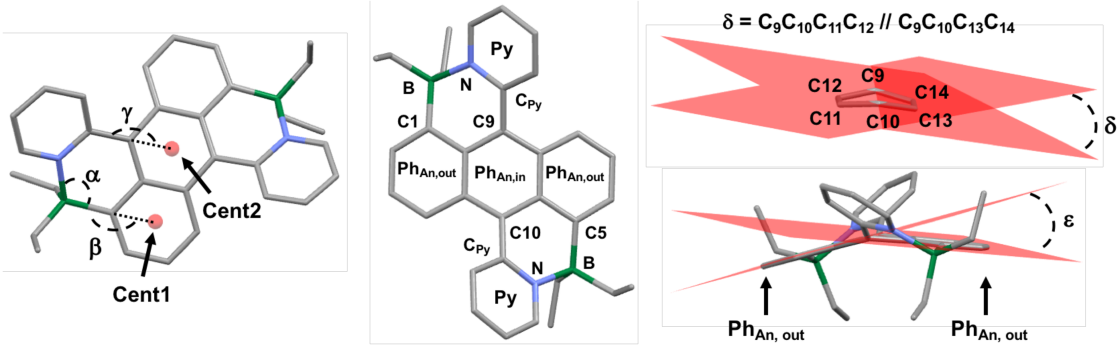

Figure 3. Illustration of geometric parameters discussed for BN-anthracenes.

The effects on the electronic structure were assessed by examining the HOMO-LUMO energy levels (Figure 4). The electron-donating effect of the Me groups raises the HOMO and LUMO levels relative to the parent molecule **BDPA**. The LUMOs are very similar in energy, except for that the methyl groups in *ortho*-position to N (**BDPA-2Me**) raise the energy. Larger differences are found in the HOMO energies. Again, the methyl groups in *ortho*-position to N in **BDPA-2Me** lead to a significant elevation of the HOMO energy level. The methyl group in *ortho*-position to the anthracene moiety lowers the HOMO energy level and, consequently, the HOMO-LUMO gap is the largest for **BDPA-5Me** (2.42 eV). The increased HOMO-LUMO gap for **BDPA-5Me** is likely related to the severe structural distortions discussed earlier that limit π-conjugation.

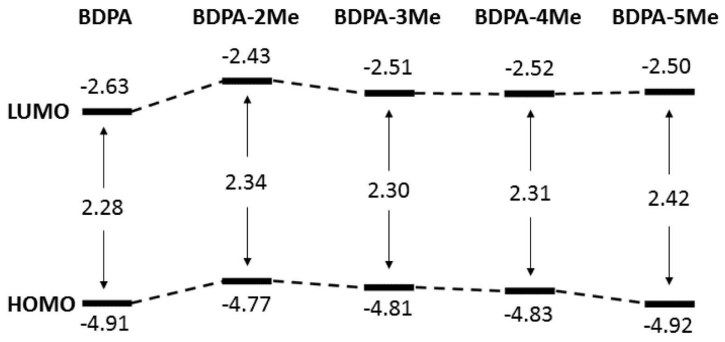

Figure 4. Comparison of HOMO and LUMO energies of BN-anthracenes

The BN-fused systems **BDPA-3Me**, **BDPA-4Me** and **BDPA-5Me** were synthesized using a similar procedure to that previously reported for compound **BDPA-2Me** (Scheme 1). The dipyridylanthracene precursors **DPA-3Me**, **DPA-4Me**, and **DPA-5Me** were obtained in 86%, 72%, and 77% yield by Suzuki-Miyaura coupling of 9,10-bis(pinacolboryl)anthracene with the respective brominated methylpyridine derivative. For **DPA-3Me** a 2.1:1 mixture of isomers and for **DPA-4Me** a 2.7:1 mixture of isomers with the pyridyl groups in a *trans* or *cis*-arrangement was found, whereas the dipyridylanthracene **DPA-5Me** was obtained as a single isomer,

presumably the sterically more favorable *trans*-derivative. Lewis base-directed electrophilic aromatic borylation with BCl_3 and $AlCl_3$ in the presence of 2,6-di-tert-butylpyridine (DBP)[7g, 24] and subsequent treatment with diethylzinc gave **BDPA-3Me** in 12%, **BDPA-4Me** in 42%, and **BDPA-5Me** in 31% yield. The products were isolated by recrystallization from CH_2Cl_2/hexanes and fully characterized by multinuclear NMR and high-resolution MALDI-TOF MS. The ^{11}B NMR signals at -0.3 ppm (**BDPA-3Me**), -0.6 ppm (**BDPA-4Me**) and -0.7 ppm (**BDPA-5Me**) are slightly shifted upfield compared with that of **BDPA-2Me** (2.8 ppm), consistent with a stronger B←N interaction. The ^1H NMR data are in good agreement with the proposed structures and all the protons could be assigned by H,H-COSY and H,H-NOESY 2D NMR analyses (Supp. Information).

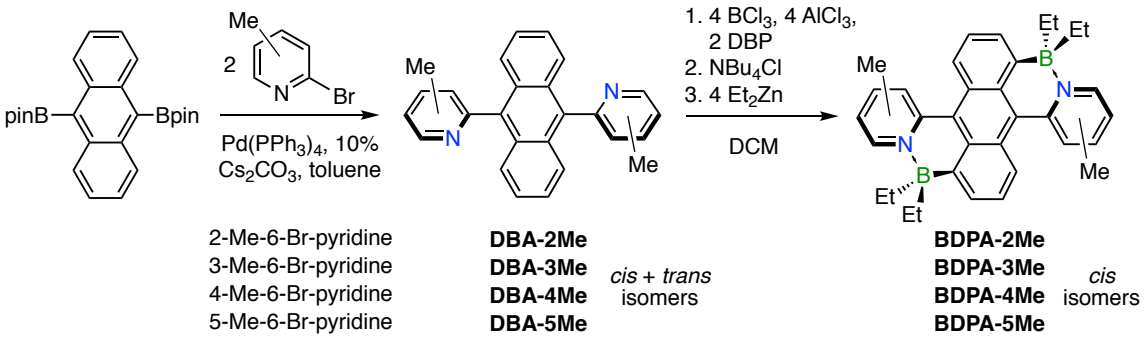

Scheme 1. Synthesis of BN-Fused 9,10-Dipyridylanthracenes.

Single crystals of **BDPA-4Me** and **BDPA-5Me** were grown from CH_2Cl_2/hexanes mixture at -20 ºC. The molecular structures are depicted in Figure 5 and the structural data summarized in Table S2. Compared with **BDPA-2Me**,[22] the B-N distances for **BDPA-4Me** and **BDPA-5Me** are significantly shorter, ranging from 1.628(8)–1.635(8) Å for **BDPA-4Me** and 1.637(2)–1.642(2) Å for **BDPA-5Me** (cf. **BDPA-2Me** 1.671(4)–1.685(3) Å), as expected for a stronger Lewis acid-base interaction. The molecular structures of **BDPA-4Me** and **BDPA-5Me** further confirm the

predicted buckled anthracene backbone with interplanar angles between the outer benzene rings of ε = 17.4° for **BDPA-4Me** and ε = 20.7° for **BDPA-5Me**. They are slightly smaller than that of **BDPA-2Me** (ε = 21.5°), which may suggest less distortion. However, an increased strain is evident from the dislocation of the boron atom from the plane of the anthracene backbone. The Cent1-$C_{1,5}$-B angles of β = 168.8, 170.5° for **BDPA-4Me** and β = 168.0, 168.8° for **BDPA-5Me** reveal much more pronounced distortions than for **BDPA-2Me** (β = 173.6, 174.8°). The steric effects of the 5-Me groups in **BDPA-5Me** also lead to the largest interplanar angle between anthracene and pyridyl (41.6 and 43.5°). Overall, these observations are consistent with the results of the DFT calculations, which suggested that shorter B-N distances result in enhanced steric strain and the presence of the Me group in 5-position in the most severe distortions.

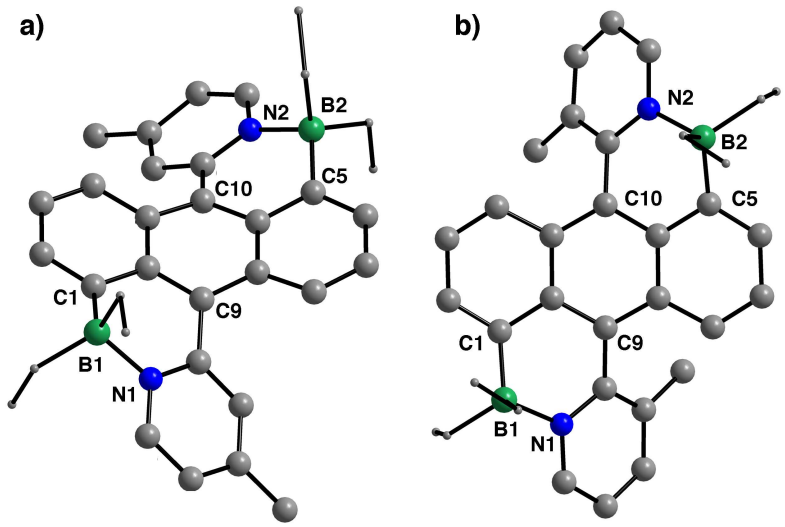

Figure 5. Ball-and-stick illustrations of the X-ray structures of a) **BDPA-4Me** and b) **BDPA-5Me**.

The crystal structures confirm the formation of the *cis*-isomer with the pyridyl groups positioned on the same side relative to the anthracene backbone. However, our prior studies revealed that, while the *trans*-isomer is higher in energy, it may be involved as an intermediate in the

interconversion of the *cis*-isomer, a process that can be monitored by the chemical exchange of the inequivalent ethyl substituents on boron. To further investigate this aspect, we performed VT ^{1}H NMR experiments that provide the free energy barrier to interconversion of the ethyl groups (Figures S2). From the coalescence temperatures the barrier was determined to $\Delta G^{\neq} = 68.5 \pm 0.7$ kJ mol^{-1} for **BDPA-2Me**, 60.8 ± 0.6 kJ mol^{-1} for **BDPA-3Me**, and 61.9 ± 0.7 kJ mol^{-1} for **BDPA-4Me** (Table S3), whereas for **BDPA-5Me** the barrier proved to be too high to observe any isomerization. Thus, despite the shorter B-N distances, the smallest energy barriers are found for **BDPA-3Me** and **BDPA-4Me**, and this indicates that the reorientation (rotation) of the pyridyl group is rate determining rather than the B-N bond cleavage.

Formation of the B←N Lewis pairs results in strong bathochromic shifts of the absorption and emission bands relative to those of the 9,10-dipyridylanthracene precursors. The BN-fused species are obtained as red crystalline solids that display a very intense orange emission in solution. A comparison of the absorption and emission spectra in CH_2Cl_2 is displayed in Figure 6 and the photophysical properties are summarized in Table 2. The longer wavelength absorption maxima for **BDPA-3Me** (555 nm) and **BDPA-4Me** (554 nm) in comparison to **BDPA-2Me** (538 nm) and **BDPA-5Me** (535 nm) are consistent with our DFT data, which showed that the relatively larger HOMO-LUMO energy gap for **BDPA-2Me** is due primarily to an increase in the LUMO energy. The larger HOMO-LUMO energy gap for **BDPA-5Me** is owing to a lower HOMO energy level. The quantum yields are consistently very high, despite the relatively low energy of the emission, with the largest value determined for **BDPA-4Me** (60%), closely followed by **BDPA-5Me** (55%), **BDPA-2Me** (53%), and **BDPA-3Me** (43%). The fluorescence lifetimes are very similar to one another, in the range of 10.2 to 11.5 ns, and significantly longer than for the non-borylated

precursors. These data are consistent with relatively small non-radiative decay constants (k_{nr}) due to the more rigid molecular framework.

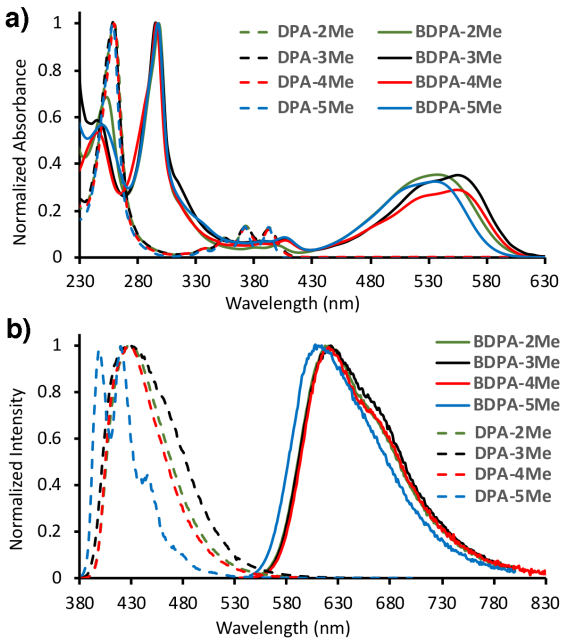

Figure 6. a) UV-vis absorption and b) emission spectra in CH_2Cl_2 solution.

Table 2. Comparison of photophysical data of BN-functionalized anthracenes and their ligand precursors

Compound	λ_{abs} [a] [nm]	$\lambda_{abs,\ TDDFT}$ [nm]	λ_{Fl} [b] [nm]	τ_{Fl} [c] [ns]	Φ_{Fl} [d]	k_r / k_{nr} [e] [10^7 s^{-1}]
DPA-2Me[22]	393, 372, 354, 259	359	428	6.0 (χ^2 = 1.64)	0.77	12.8 / 3.8
DPA-3Me	393, 372, 354, 259	361	427	5.9 (χ^2 = 1.46)	0.59	10.0 / 6.9
DPA-4Me	393, 372, 354, 259	359	428	6.1 (χ^2 = 1.42)	0.64	10.5 / 5.9
DPA-5Me	392, 372, 354, 258	355	419, 397	6.9 (χ^2 = 1.42)	0.60	8.7 / 5.8
BDPA-2Me[22]	538, 298, 293	523	620	11.1 (χ^2 = 1.54)	0.53	4.8 / 4.2
BDPA-3Me	555, 528 (sh), 295	532	622	10.2 (χ^2 = 1.53)	0.43	4.2 / 5.6
BDPA-4Me	554, 525 (sh), 298	533	621	10.9 (χ^2 = 2.33)[f]	0.60	5.5 / 3.7
BDPA-5Me	535, 297	512	612	11.5 (χ^2 = 1.50)	0.55	4.8 / 3.9

[a] In CH_2Cl_2 solution. [b] Excited at 372 nm (**DPA-2Me**, **DPA-3Me**, **DPA-4Me** and **DPA-5Me**), 538 nm (**BDPA-2Me**), 528 nm (**BDPA-3Me**), 525 nm (**BDPA-4Me**), 535 nm (**BDPA-5Me**); [c] excited with a nanoLED at 388 nm (ligands), or 450 nm (borylated species); [d] absolute quantum yield determined using an integrating sphere; [e] radiative (k_r) and non-radiative (k_{nr}) decay rate constants are calculated using the equations $k_r = \Phi / \tau$, $k_{nr} = (1 - \Phi) / \tau$; [f] for double-exponential fit: τ_{Fl} = 1.3 ns (3%), 11.1 ns (97%) (χ^2 = 1.62).

Cyclic (CV) and square wave voltammetry (SWV) data acquired in THF containing 0.1 M $Bu_4N[PF_6]$ show two consecutive reversible reduction processes (Figure S3). As predicted by the DFT calculations, the first reduction occurs slightly more readily for **BDPA-3Me** (E_{red} = −1.77 V vs. $Fc^{+/0}$), **BDPA-4Me** (E_{red} = −1.77 V) and **BDPA-5Me** (E_{red} = −1.81 V) in comparison with **BDPA-2Me** (E_{red} = −1.87 V) (Table 3). Of note is that the second reduction occurs at a much more negative potential for **BDPA-5Me** in comparison to the other isomers, resulting in an unusually large redox splitting of ΔE = 0.38 V. Considering that the LUMO orbitals show a quinoidal π-delocalization between the anthracene and pyridyl groups, this may be due to steric constraints that hinder the planarization of the pyridyl and anthracene groups in **BDPA-5Me**. Oxidative scans performed in CH_2Cl_2 containing 0.1 M $Bu_4N[PF_6]$ show irreversible waves with peak potentials of E_{pa} = 0.40 V (**BDPA-2Me**), 0.39 V (**BDPA-3Me**), 0.42 V (**BDPA-4Me**), and 0.48 V (**BDPA-5Me**) (Figure S3). The derived electrochemical HOMO–LUMO gaps range from 2.16 eV (**BDPA-3Me**) to 2.29 eV (**BDPA-5Me**), in excellent agreement with the trends in the optical gaps deduced from the UV-vis absorption spectra.

Table 3. Electrochemical data of BN-functionalized anthracenes and comparison of HOMO-LUMO gaps with results from DFT calculations and UV-vis absorption spectroscopy

Compound	$E_{ox}^{CV\,[a]}$ [V]	$E_{red}^{CV\,[b]}$ [V]	HOMO[c] [eV]	LUMO[c] [eV]	$E_g^{CV\,[c]}$ [eV]	$E_g^{DFT[d]}$ [eV]	$E_{g,}^{opt\,[e]}$ [eV]
BDPA-2Me[22]	0.40	-1.87, -2.07	-5.20	-2.93	2.27	2.34	2.30
BDPA-3Me	0.39	-1.77, -2.02	-5.19	-3.03	2.16	2.30	2.23
BDPA-4Me	0.42	-1.77, -2.00	-5.22	-3.03	2.19	2.31	2.24
BDPA-5Me	0.48	-1.81, -2.19	-5.28	-2.99	2.29	2.42	2.32

[a] Recorded using 0.1M $Bu_4N[PF_6]$ in CH_2Cl_2, $E_{ox} = E_{pa}$; [b] recorded using 0.1M $Bu_4N[PF_6]$ in THF, $E_{red} = 0.5\ (E_{pc} + E_{pa})$; [c] determined from CV data using the equations $E_{LUMO} = -(4.8 + E_{red})$ and $E_{HOMO} = -(4.8 + E_{ox})$; [d] from DFT calculations at the rb3lyp/6-31g(d) level of theory; [e] estimated from absorption maxima in CH_2Cl_2 solution.

Beyond the superior emissive properties, an intriguing characteristic of anthracenes is their ability to take up and release singlet oxygen via the reversible formation of endoperoxides. This behavior in not only of key importance to cancer treatment via photodynamic therapy,[12-13] but has also been exploited in materials science, for instance, in photolithography,[14] fluorescent anti-counterfeiting[15], and the development of molecular switches[16]. Typically, an external sensitizer is added to promote the conversion of triplet to singlet oxygen, which in turn reacts with the acene to yield the respective endoperoxides. In a very recent study Linker demonstrated that this is also the case for dipyridylanthracenes which are converted to the endoperoxides by sensitization with tetraphenylporphyrin.[25] While spontaneous self-sensitized reaction of higher acenes (e.g. pentacene) with oxygen is frequently encountered, relative few examples of anthracene derivatives are known that display efficient self-sensitized endoperoxide formation with visible light, most notably systems in which the phenyl groups in 9,10-diphenylanthracene are fused to the anthracene backbone via O, S, C=O, or aryl bridges that results in planarized structures and red-shifted

absorptions.[26] We found that the BN-functionalized anthracenes rapidly react with O_2 in the presence of visible light to selectively form the corresponding endoperoxide **BPO-2Me**, **BPO-3Me**, **BPO-4Me**, and **BPO-5Me** (Figure 7). The endoperoxides were fully characterized by multinuclear NMR and high-resolution MALDI-TOF MS (SI).

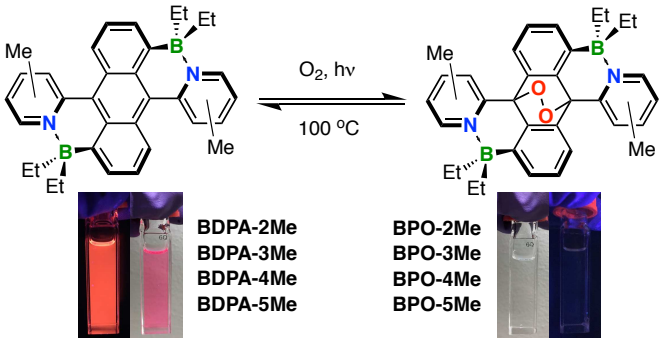

Figure 7. Self-sensitized formation of endoperoxides and photographs under ambient light and UV-irradiation illustrating color changes for the reversible conversion of **BDPA-5Me** to its endoperoxide **BPO-5Me**.

To explore differences in reactivity, solutions of the acenes in oxygen-saturated CH_2Cl_2 (1×10^{-5} M) were irradiated with a Xe lamp at room temperature (Figure 8a, see SI for details). The kinetic data reveal a strong influence of substituent effects on the reactivity as **BDPA-5Me** with the Me groups in close proximity to the anthracene backbone reacts almost an order of magnitude more slowly than the other derivatives to give the corresponding endoperoxide **BPO-5Me**. In the case of diarylanthracenes, zwitterionic intermediates consisting of a C-9 attached peroxo anion and C10-centered carbocation have been proposed, and a correlation between the HOMO energy of diarylanthrancenes with their reactivity towards O_2 has been postulated.[27] According to our calculations the HOMO level decreases slightly in the order of **BDPA-2Me** > **BDPA-3Me** ≈ **BDPA-4Me** > **BDPA-5Me** (Figure 4), which is consistent with their relative reactivity except for

that **BDPA-2Me** reacts at a similar rate as **BDPA-3Me** and **BDPA-4Me**. However, the much lower rate for **BDPA-5Me** suggests that steric factors play a major role, most likely by preventing further planarization of the pyridyl group and the anthracene backbone, which is necessary to stabilize the proposed carbocation intermediate[27] in the peroxo intermediate for **BDPA-5Me** (Figure 8a). On the other hand, the fact that the rate for **BDPA-2Me** is similar to that of **BDPA-3Me** and **BDPA-4Me** suggests that the effect of the steric pressure of the Me group in 2-position and the ensuing weakening of the B←N interaction is less significant as it does not affect the ability of the pyridyl group to adopt a position that is coplanar with the anthracene backbone.

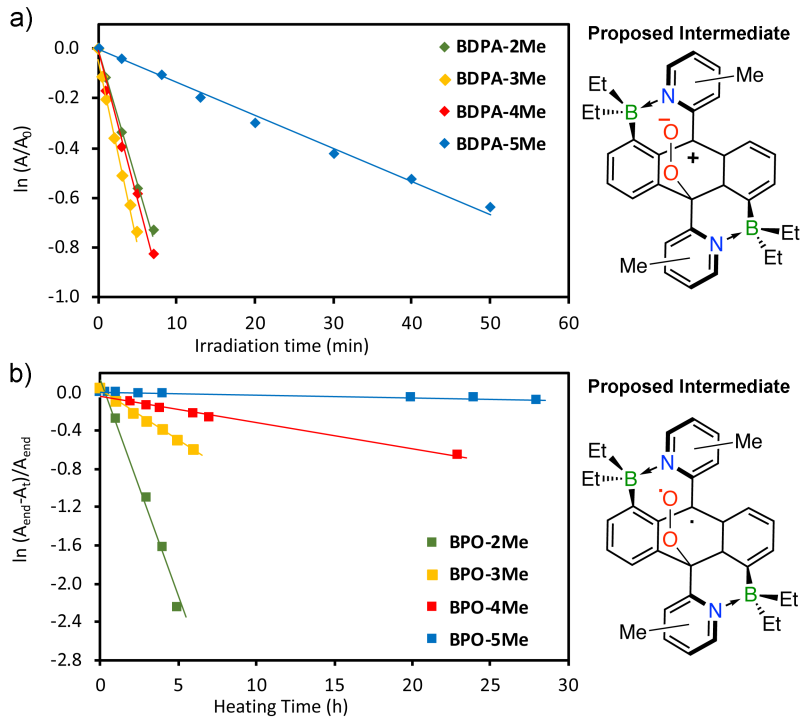

Figure 8. a) Pseudo first-order kinetics and structures of proposed intermediates for the reaction of BN-functionalized anthracenes with oxygen upon photoirradiation with a Xe lamp in CH_2Cl_2 solution (**BDPA-2Me**: $k = 1.8 \times 10^{-3}$ s^{-1}, **BDPA-3Me**: $k = 2.4 \times 10^{-3}$ s^{-1}, **BDPA-4Me**: 2.0×10^{-3} s^{-1}, **BDPA-5Me:** 2.2×10^{-4} s^{-1}). b) Kinetics for the thermolysis of the endoperoxides at 100 ºC and structures of proposed intermediates; A_{end}: final absorption intensity of BDPA, A_t: absorption intensity of BDPA at a given time (**BPO-2Me**: $k = 1.2 \times 10^{-4}$ s^{-1}, **BPO-3Me**: 2.9×10^{-5} s^{-1}, **BPO-4Me**: 7.6×10^{-6} s^{-1}, **BPO-5Me:** 7.5×10^{-7} s^{-1}).

Another appealing aspect of diarylanthracene endoperoxides is their ability to thermally revert to the parent acenes with generation of singlet oxygen that can be delivered on demand.[11b, 11c] This process is believed to proceed through a diradical intermediate generated upon initial cleavage of one of the C-O bonds.[27] Indeed, when heated to 100 ºC in toluene, the BPOs gradually revert back to the parent acenes (Figure 8b). The rate of cyclo-reversion for **BPO-2Me** is by far the highest, almost an order of magnitude higher than that of **BPO-3Me** and more than two orders of magnitude higher than that of **BPO-5Me**. This suggests a relatively lower kinetic barrier for **BPO-2Me** and is in good agreement with the calculated C-O and O-O bond distances for the BPOs which increase in the order of **BPO-5Me** < **BPO-4Me** ≈ **BPO-3Me** < **BPO-2Me** (Table S11). While not directly correlated, our results are also consistent with a comparison of the relative stability of the BN-anthracenes and their endoperoxides, where the regeneration of **BDPA-5Me** from its endoperoxide **BPO-5Me** is energetically least favorable (Table 4). **BDPA-2Me** is highest in energy among the acenes, presumably due to the weaker B←N interaction (B-N 1.690 Å), but the formation of its endoperoxide **BPO-2Me** is predicted to be relatively even less favorable (B-N 1.727, 1.745 Å). The elongated B-N bond distances for **BPO-2Me** and expected more facile bond dissociation could also be an indication that generation of a tricoordinate borane plays a role in promoting the release of oxygen from **BPO-2Me**. Indeed, the rate of cyclo-reversion for **BPO-2Me** ($t_{1/2}$ = 105 mins) is higher than that reported for diphenylanthracene ($t_{1/2}$ = 121 mins) and, interestingly, the parent non-borylated di-*o*-pyridylanthracene was reported to only release O_2 at a temperature of 135 ºC at which other side reactions occur.[25, 27a] In a recent study, Linker and coworkers proposed that N-methylation of di(*o*-pyridyl)anthracene triggers very rapid O_2 release by interaction of the cationic methylpyridinium group with the peroxo bridge.[28] Although a direct interaction between the Lewis acidic boron center generated upon B-N cleavage and the peroxo bridge is sterically not feasible,

it is conceivable that the borane interacts with a lone pair on the peroxo group after the initial C-O bond cleavage.

Table 4. Relative computed energies for isomeric BN-anthracenes and their endoperoxides[a]

	ΔE_{BDPA} [b] (kJ/mol)	ΔE_{BPO} [c] (kJ/mol)	$\Delta(E_{BPO} - E_{BDPA})$ (kJ/mol)
BDPA-2Me	+77.8	+99.4	+21.6
BDPA-3Me	+5.9	+28.1	+22.2
BDPA-4Me	≡ 0	≡ 0	≡ 0
BDPA-5Me	+52.6	+40.0	-12.6

[a] Optimized at rb3lyp/6-31g(d) level of theory. [b] Comparison of total energy relative to sterically unhindered 4-methylated acene. [c] Comparison of total energy relative to sterically unhindered 4-methylated acene endoperoxide.

The results described above indicate that while compound **BDPA-2Me** reacts similarly fast as **BDPA-3Me** and **BDPA-4Me** with O_2 under photoirradiation it thermally releases singlet O_2 more readily. On the other, **BDPA-5Me** sluggishly reacts with O_2 and only very slowly releases singlet O_2. This suggests that by simply varying the substitution pattern on the pyridyl moiety either a material (**BDPA-2Me**) that can be used for delivery of singlet oxygen on demand or a material (**BDPA-5Me**) that acts as a singlet oxygen sensitizer for oxygenation of other compounds can be achieved. To test the ability of the BN-fused dipyridylanthracenes to act as a singlet oxygen sensitizer and promote oxygenation of other substrates we performed competition experiments with 9,10-dimethylanthracene (DMA) as a singlet oxygen acceptor. Indeed, all the compounds promote oxygenation of DMA as evidenced by a decrease in the characteristic absorptions between 300 to 400 nm. However, whereas **BDPA-2Me**, **BDPA-3Me** and **BDPA-4Me** undergo preferential self-sensitized oxygenation and the oxygenation of DMA occurs at a relatively lower rate (Figure S7), **BDPA-5Me** leads to preferential conversion of DMA into its endoperoxide. The oxidation of

DMA using 10% of **BDPA-5Me** as a photosensitizer is illustrated in Figure 9. In the absence of **BDPA-5Me** as a photosensitizer only negligible amounts of DMA are converted upon photoirradiation under otherwise identical conditions.

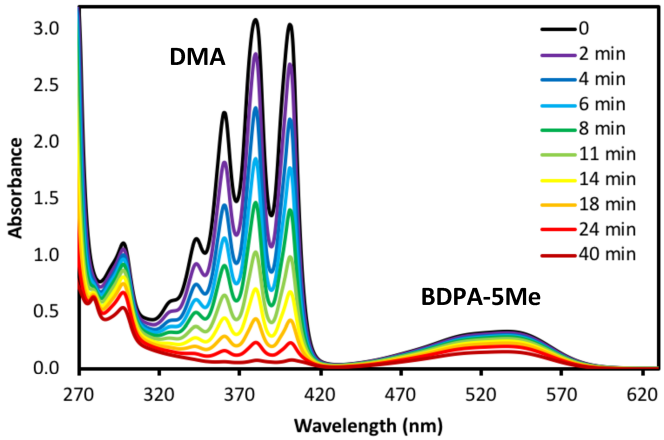

Figure 9. Photoirradiation of 9,10-dimethylanthracene (DMA) in the presence of 10 mol% **BDPA-5Me** with a Xe lamp in oxygen-saturated CH_2Cl_2 solution followed by UV-Vis spectroscopy.

Conclusions

We have synthesized a series of BN-fused 9,10-dipyridylanthracenes with Me groups in different positions of the pyridyl ring to investigate in detail steric and electronic effects on the structural parameters, the optical and electronic properties, and the reactivity towards oxygen. Single crystal X-ray structures and DFT calculations reveal the most pronounced structural distortions for **BDPA-5Me** as reflected in a strong buckling and dislocation of the boron atoms from the anthracene backbone, whereas for **BDPA-2Me** a lengthening of the B-N bonds allows for some relaxation of the overall steric strain. The dynamic nature of the B←N Lewis pair formation was

verified by variable temperature NMR spectroscopy and the barrier to the structural inversion correlated to the hindered rotation of the pyridyl group relative to the anthracene backbone. The substitution pattern also influences the HOMO and LUMO energy levels as evidenced by electrochemical, UV-Vis and fluorescence spectroscopy measurements. The most dramatic effect of the substitution pattern is seen in the reactivity toward oxygen to give the respective endoperoxides and their cyclo-reversion with release of singlet oxygen. **BDPA-2Me**, **BDPA-3Me** and **BDPA-4Me** rapidly react with O_2 under photoirradiation, whereas the rate for **BDPA-5Me** is one order of magnitude lower. The difference in reactivity is attributed to kinetic factors where the Me groups in 5-position prevent effective planarization and therefore limit carbocation stabilization of the generally accepted zwitterionic intermediate in the oxygenation reaction. The substitution pattern also has a dramatic effect on the rate of thermal release of singlet oxygen from the endoperoxides with almost an order of magnitude difference in reactivity between each compound, **BDPA-5Me** < **BDPA-4Me** < **BDPA-3Me** < **BDPA-2Me**. We speculate that the much higher rate of cyclo-reversion for **BDPA-2Me** may relate to the weaker B←N dative bond and possibly an involvement of the borane Lewis acid sites in stabilizing the radical intermediate.

The demonstrated ability to alter the reactivity of the BN-anthracenes through relatively minor structural modifications has important ramifications in respect to potential applications as singlet oxygen sensitizers and on-demand delivery of singlet oxygen from the respective endoperoxides. With respect to singlet oxygen sensitization it is desirable to avoid self-sensitized reactivity with formation of endoperoxides. Our studies clearly indicate that further enhanced bulk in 5-position will be beneficial in this respect. A lower reactivity towards oxygen is also beneficial for applications in organic electronics and fluorescent imaging. Conversely, a high propensity for self-sensitized endoperoxide formation and subsequent cyclo-reversion is of interest for on-

demand delivery of singlet O_2. In this respect, the favorable reactivity of **BDPA-2Me** suggests that further weakening of the B-N bond, possibly even a fully ring-opened "frustrated" Lewis pair structure, could provide superior singlet oxygen release properties and might also result in unusual reactivity toward other substrates.

Acknowledgements. This material is based upon work supported by the US National Science Foundation (NSF) under Grant CHE-1664975. A 500 MHz NMR spectrometer (MRI 1229030) and an X-ray diffractometer (CRIF 0443538) were purchased with support from the NSF and Rutgers University.

Electronic Supplementary Information (ESI) available: Details on the synthesis and characterization, NMR and mass spectral data of all new compounds, VT NMR data, X-ray crystal structure plots showing intermolecular interactions, photophysical and electrochemical data, results from DFT and TD-DFT calculations. Crystal structure data (cif). See DOI: 10.1039/x0xx00000x

References

1. (a) He, X. M.; Baumgartner, T., Conjugated main-group polymers for optoelectronics. *RSC Adv.* **2013**, *3*, 11334-11350; (b) Priegert, A. M.; Rawe, B. W.; Serin, S. C.; Gates, D. P., Polymers and the p-block elements. *Chem. Soc. Rev.* **2016**, *45*, 922-953; (c) Stępień, M.; Gońka, E.; Żyła, M.; Sprutta, N., Heterocyclic Nanographenes and Other Polycyclic Heteroaromatic Compounds: Synthetic Routes, Properties, and Applications. *Chem. Rev.* **2017**, *117*, 3479–3716; (d) Zhang, G. Y.; Zhao, J. B.; Chow, P. C. Y.; Jiang, K.; Zhang, J. Q.; Zhu, Z. L.; Zhang, J.; Huang, F.; Yan, H., Nonfullerene Acceptor Molecules for Bulk Heterojunction Organic Solar Cells. *Chem. Rev.* **2018**, *118*, 3447-3507; (e) Gon, M.; Tanaka, K.; Chujo, Y., Recent progress in the development of advanced element-block materials. *Polym. J.* **2018**, *50*, 109-126; (f) Baumgartner, T.; Jäkle, F., *Main group strategies towards functional hybrid materials*. John Wiley & Sons: Hoboken, NJ, 2018; p pages cm; (g) Vidal, F.; Jäkle, F., Functional Polymeric Materials Based on Main Group Elements. *Angew. Chem. Int. Ed.* **2019**, *58*, 5846-5870.

2. (a) Entwistle, C. D.; Marder, T. B., Applications of Three-Coordinate Organoboron Compounds and Polymers in Optoelectronics. *Chem. Mat.* **2004**, *16*, 4574-4585; (b) Jäkle, F., Advances in the Synthesis of Organoborane Polymers for Optical, Electronic and Sensory Applications. *Chem. Rev.* **2010**, *110*, 3985-4022; (c) Escande, A.; Ingleson, M. J., Fused polycyclic aromatics incorporating boron in the core: fundamentals and applications. *Chem. Commun.* **2015**, *51*, 6257-6274; (d) Wakamiya, A.; Yamaguchi, S., Designs of Functional pi-Electron Materials based on the Characteristic Features of Boron. *B. Chem. Soc. Jpn.* **2015**, *88*, 1357-1377; (e) Wang, X. Y.; Wang, J. Y.; Pei, J., BN Heterosuperbenzenes: Synthesis and Properties. *Chem. Eur. J.* **2015**, *21*, 3528-3539; (f) Ji, L.; Griesbeck, S.; Marder, T. B., Recent developments in and perspectives on three-coordinate boron materials: a bright future. *Chem. Sci.* **2017**, *8*, 846-863; (g) Giustra, Z. X.; Liu, S. Y., The State of the Art in Azaborine Chemistry: New Synthetic Methods and Applications. *J. Am. Chem. Soc.* **2018**, *140*, 1184-1194; (h) von Grotthuss, E.; John, A.; Kaese, T.; Wagner, M., Doping Polycyclic Aromatics with Boron for Superior Performance in Materials Science and Catalysis. *Asian J. Org. Chem.* **2018**, *7*, 37-53; (i) Huang, J. H.; Li, Y. Q., BN Embedded Polycyclic pi-Conjugated Systems: Synthesis, Optoelectronic Properties, and Photovoltaic Applications. *Front. Chem.* **2018**, *6*; (j) Saito, S.; Matsuo, K.; Yamaguchi, S., Polycyclic pi-Electron System with Boron at Its Center. *J. Am. Chem. Soc.* **2012**, *134*, 9130-9133; (k) Reus, C.; Weidlich, S.; Bolte, M.; Lerner, H. W.; Wagner, M., C-Functionalized, Air- and Water-Stable 9,10-Dihydro-9,10-diboraanthracenes: Efficient Blue to Red Emitting Luminophores. *J. Am. Chem. Soc.* **2013**, *135*, 12892-12907; (l) Neue, B.; Araneda, J. F.; Piers, W. E.; Parvez, M., BN-Dibenzo[a,o]picenes: Analogues of an Unknown Polycyclic Aromatic Hydrocarbon. *Angew. Chem. Int. Ed.* **2013**, *52*, 9966-9969; (m) Sarkar, S. K.; Mukherjee, S.; Thilagar, P., Going beyond Red with a Tri- and Tetracoordinate Boron Conjugate: Intriguing Near-IR Optical Properties and Applications in Anion Sensing. *Inorg. Chem.* **2014**, *53*, 2343-2345; (n)

Wang, X. Y.; Zhuang, F. D.; Wang, R. B.; Wang, X. C.; Cao, X. Y.; Wang, J. Y.; Pei, J., A Straightforward Strategy toward Large BN-Embedded pi-Systems: Synthesis, Structure, and Optoelectronic Properties of Extended BN Heterosuperbenzenes. *J. Am. Chem. Soc.* **2014**, *136*, 3764-3767; (o) Levine, D. R.; Siegler, M. A.; Tovar, J. D., Thiophene-Fused Borepins As Directly Functionalizable Boron-Containing pi-Electron Systems. *J. Am. Chem. Soc.* **2014**, *136*, 7132-7139; (p) Kushida, T.; Shuto, A.; Yoshio, M.; Kato, T.; Yamaguchi, S., A Planarized Triphenylborane Mesogen: Discotic Liquid Crystals with Ambipolar Charge-Carrier Transport Properties. *Angew. Chem. Int. Ed.* **2015**, *54*, 6922-6925; (q) Yin, X. D.; Liu, K. L.; Ren, Y.; Lalancette, R. A.; Loo, Y. L.; Jäkle, F., Pyridalthiadiazole acceptor-functionalized triarylboranes with multi-responsive optoelectronic characteristics. *Chem Sci* **2017**, *8*, 5497-5505; (r) Yang, Z. Y.; Mao, Z.; Xie, Z. L.; Zhang, Y.; Liu, S. W.; Zhao, J.; Xu, J. R.; Chi, Z. G.; Aldred, M. P., Recent advances in organic thermally activated delayed fluorescence materials. *Chem. Soc. Rev.* **2017**, *46*, 915-1016; (s) Meng, B.; Ren, Y.; Liu, J.; Jäkle, F.; Wang, L. X., p-pi Conjugated Polymers Based on Stable Triarylborane with n-Type Behavior in Optoelectronic Devices. *Angew. Chem. Int. Ed.* **2018**, *57*, 2183-2187; (t) Cai, X. Y.; Su, S. J., Marching Toward Highly Efficient, Pure-Blue, and Stable Thermally Activated Delayed Fluorescent Organic Light-Emitting Diodes. *Adv. Funct. Mater.* **2018**, *28*; (u) John, A.; Bolte, M.; Lerner, H. W.; Meng, G. Y.; Wang, S. N.; Peng, T.; Wagner, M., Doubly boron- doped pentacenes as emitters for OLEDs. *J. Mater. Chem. C* **2018**, *6*, 10881-10887; (v) Wu, T. L.; Huang, M. J.; Lin, C. C.; Huang, P. Y.; Chou, T. Y.; Chen-Cheng, R. W.; Lin, H. W.; Liu, R. S.; Cheng, C. H., Diboron compound-based organic light-emitting diodes with high efficiency and reduced efficiency roll-off. *Nat. Photonics* **2018**, *12*, 235; (w) Liang, X.; Yan, Z. P.; Han, H. B.; Wu, Z. G.; Zheng, Y. X.; Meng, H.; Zuo, J. L.; Huang, W., Peripheral Amplification of Multi-Resonance Induced Thermally Activated Delayed Fluorescence for Highly Efficient OLEDs. *Angew. Chem. Int. Ed.* **2018**, *57*, 11316-11320.

3. (a) Ma, K.; Scheibitz, M.; Scholz, S.; Wagner, M., Applications of boron-nitrogen and boron-phosphorus adducts in organometallic chemistry. *J. Organomet. Chem.* **2002**, *652*, 11-19; (b) Li, D.; Zhang, Z. L.; Zhao, S. S.; Wang, Y.; Zhang, H. Y., Diboron-containing fluorophores with extended ladder-type pi-conjugated skeletons. *Dalton Trans.* **2011**, *40*, 1279-1285; (c) Cao, Y.; Nagle, J. K.; Wolf, M. O.; Patrick, B. O., Tunable Luminescence of Bithiophene-Based Flexible Lewis Pairs. *J. Am. Chem. Soc.* **2015**, *137*, 4888-4891; (d) Dou, C. D.; Ding, Z. C.; Zhang, Z. J.; Xie, Z. Y.; Liu, J.; Wang, L. X., Developing Conjugated Polymers with High Electron Affinity by Replacing a C-C Unit with a B - N Unit. *Angew. Chem. Int. Ed.* **2015**, *54*, 3648-3652; (e) Yusuf, M.; Liu, K. L.; Guo, F.; Lalancette, R. A.; Jäkle, F., Luminescent organoboron ladder compounds via directed electrophilic aromatic C-H borylation. *Dalton Trans.* **2016**, *45*, 4580-4587; (f) Zhu, C. Z.; Guo, Z. H.; Mu, A. U.; Liu, Y.; Wheeler, S. E.; Fang, L., Low Band Gap Coplanar Conjugated Molecules Featuring Dynamic Intramolecular Lewis Acid-Base Coordination. *J. Org. Chem.* **2016**, *81*, 4347-4352; (g) Shimogawa, H.; Yoshikawa, O.; Aramaki, Y.; Murata, M.; Wakamiya, A.; Murata, Y., 4,7-Bis[3-(dimesitylboryl)thien-2-yl]benzothiadiazole: Solvato-, Thermo-, and Mechanochromism Based on the Reversible Formation of an Intramolecular B-N Bond. *Chem. Eur. J.* **2017**, *23*, 3784-3791; (h) Schraff, S.; Sun, Y.; Pammer, F., Tuning of

electronic properties via labile N -> B-coordination in conjugated organoboranes. *J. Mater. Chem. C* **2017**, *5*, 1730-1741; (i) Grandl, M.; Sun, Y.; Pammer, F., Electronic and structural properties of N -> B-ladder boranes with high electron affinity. *Org. Chem. Front.* **2018**, *5*, 336-352; (j) Zhu, C. Z.; Fang, L., Locking the Coplanar Conformation of pi-Conjugated Molecules and Macromolecules Using Dynamic Noncovalent Bonds. *Macromol. Rapid Comm.* **2018**, *39*; (k) Zeng, C.; Yuan, K.; Wang, N.; Peng, T.; Wu, G.; Wang, S., The opposite and amplifying effect of B <- N coordination on photophysical properties of regioisomers with an unsymmetrical backbone. *Chem. Sci.* **2019**, *10*, 1724-1734.

4. (a) Ros, A.; Estepa, B.; Lopez-Rodriguez, R.; Alvarez, E.; Fernandez, R.; Lassaletta, J. M., Use of Hemilabile N,N Ligands in Nitrogen-Directed Iridium-Catalyzed Borylations of Arenes. *Angew. Chem. Int. Ed.* **2011**, *50*, 11724-11728; (b) Kuninobu, Y.; Iwanaga, T.; Omura, T.; Takai, K., Palladium-Catalyzed ortho-Selective C-H Borylation of 2-Phenylpyridine and Its Derivatives at Room Temperature. *Angew. Chem. Int. Ed.* **2013**, *52*, 4431-4434; (c) Keske, E. C.; Moore, B. D.; Zenkina, O. V.; Wang, R. Y.; Schatte, G.; Crudden, C. M., Highly selective directed arylation reactions via back-to-back dehydrogenative C-H borylation/arylation reactions. *Chem. Commun.* **2014**, *50*, 9883-9886; (d) Kondrashov, M.; Raman, S.; Wendt, O. F., Metal controlled regioselectivity in the cyclometallation of 2-(1-naphthyl)-pyridine. *Chem. Commun.* **2015**, *51*, 911-913.

5. Grandl, M.; Kaese, T.; Krautsieder, A.; Sun, Y.; Pammer, F., Hydroboration as an Efficient Tool for the Preparation of Electronically and Structurally Diverse N -> B-Heterocycles. *Chem.-Eur. J.* **2016**, *22*, 14373-14382.

6. (a) Ishida, N.; Moriya, T.; Goya, T.; Murakami, M., Synthesis of Pyridine-Borane Complexes via Electrophilic Aromatic Borylation. *J. Org. Chem.* **2010**, *75*, 8709-8712; (b) Wong, H.-L.; Wong, W.-T.; Yam, V. W.-W., Photochromic Thienylpyridine Bis(alkynyl)borane Complexes: Toward Readily Tunable Fluorescence Dyes and Photoswitchable Materials. *Org. Lett.* **2012**, *14*, 1862-1865; (c) Niu, L.; Yang, H.; Wang, R.; Fu, H., Metal-Free Ortho C H Borylation of 2-Phenoxypyridines under Mild Conditions. *Org. Lett.* **2012**, *14*, 2618-2621; (d) Dhanunjayarao, K.; Sa, S.; Aradhyula, B. P. R.; Venkatasubbaiah, K., Synthesis of phenanthroimidazole-based four coordinate organoboron compounds. *Tetrahedron* **2018**, *74*, 5819-5825.

7. (a) Rao, Y. L.; Amarne, H.; Wang, S. N., Photochromic four-coordinate N,C-chelate boron compounds. *Coord. Chem. Rev.* **2012**, *256*, 759-770; (b) Zhao, Z. J.; Chang, Z. F.; He, B. R.; Chen, B.; Deng, C. M.; Lu, P.; Qiu, H. Y.; Tang, B. Z., Aggregation-Induced Emission and Efficient Solid-State Fluorescence from Tetraphenylethene-Based N,C-Chelate Four-Coordinate Organoborons. *Chem. Eur. J.* **2013**, *19*, 11512-11517; (c) Rao, Y. L.; Hörl, C.; Braunschweig, H.; Wang, S. N., Reversible Photochemical and Thermal Isomerization of Azaboratabisnorcaradiene to Azaborabenzotropilidene. *Angew. Chem. Int. Ed.* **2014**, *53*, 9086-9089; (d) Baranov, M. S.; Solntsev, K. M.; Baleeva, N. S.; Mishin, A. S.; Lukyanov, S. A.; Lukyanov, K. A.; Yampolsky, I.

V., Red-Shifted Fluorescent Aminated Derivatives of a Conformationally Locked GFP Chromophore. *Chem.-Eur. J.* **2014**, *20*, 13234-13241; (e) Shaikh, A. C.; Ranade, D. S.; Thorat, S.; Maity, A.; Kulkarni, P. P.; Gonnade, R. G.; Munshi, P.; Patil, N. T., Highly emissive organic solids with remarkably broad color tunability based on N,C-chelate, four-coordinate organoborons. *Chem. Commun.* **2015**, *51*, 16115-16118; (f) Pais, V. F.; Alcaide, M. M.; Lopez-Rodriguez, R.; Collado, D.; Najera, F.; Perez-Inestrosa, E.; Alvarez, E.; Lassaletta, J. M.; Fernandez, R.; Ros, A.; Pischel, U., Strongly Emissive and Photostable Four-Coordinate Organoboron N,C Chelates and Their Use in Fluorescence Microscopy. *Chem. - Eur. J.* **2015**, *21*, 15369-15376; (g) Crossley, D. L.; Vitorica-Yrezabal, I.; Humphries, M. J.; Turner, M. L.; Ingleson, M. J., Highly Emissive Far Red/Near-IR Fluorophores Based on Borylated Fluorene-Benzothiadiazole Donor-Acceptor Materials. *Chem. Eur. J.* **2016**, *22*, 12439-12448; (h) Wong, B. Y. W.; Wong, H. L.; Wong, Y. C.; Chan, M. Y.; Yam, V. W. W., Air-Stable Spirofluorene-Containing Ladder-Type Bis(alkynyl)borane Compounds with Readily Tunable Full Color Emission Properties. *Chem.-Eur. J.* **2016**, *22*, 15095-15106; (i) Zhao, R. Y.; Dou, C. D.; Xie, Z. Y.; Liu, J.; Wang, L. X., Polymer Acceptor Based on BN Units with Enhanced Electron Mobility for Efficient All-Polymer Solar Cells. *Angew. Chem. Int. Ed.* **2016**, *55*, 5313-5317; (j) Shiu, Y. J.; Chen, Y. T.; Lee, W. K.; Wu, C. C.; Lin, T. C.; Liu, S. H.; Chou, P. T.; Lu, C. W.; Cheng, I. C.; Lien, Y. J.; Chi, Y., Efficient thermally activated delayed fluorescence of functional phenylpyridinato boron complexes and high performance organic light-emitting diodes. *J. Mater. Chem. C* **2017**, *5*, 1452-1462; (k) Matsuo, K.; Yasuda, T., Enhancing thermally activated delayed fluorescence characteristics by intramolecular B-N coordination in a phenylpyridine-containing donor-acceptor pi-system. *Chem. Commun.* **2017**, *53*, 8723-8726; (l) Hecht, R.; Kade, J.; Schmidt, D.; Nowak-Krol, A., n-Channel Organic Semiconductors Derived from Air-Stable Four-Coordinate Boron Complexes of Substituted Thienylthiazoles. *Chem.-Eur. J.* **2017**, *23*, 11620-11628; (m) Mellerup, S. K.; Li, C.; Peng, T.; Wang, S. N., Regioselective Photoisomerization/C-C Bond Formation of Asymmetric B(ppy)(Mes)(Ar): The Role of the Aryl Groups on Boron. *Angew. Chem. Int. Ed.* **2017**, *56*, 6093-6097; (n) Alahmadi, A. F.; Lalancette, R. A.; Jäkle, F., Highly Luminescent Ladderized Fluorene Copolymers Based on B-N Lewis Pair Functionalization. *Macromol. Rapid Comm.* **2018**, *39*; (o) Stanoppi, M.; Lorbach, A., Boron-based donor-spiro-acceptor compounds exhibiting thermally activated delayed fluorescence (TADF). *Dalton Trans.* **2018**, *47*, 10394-10398; (p) Mellerup, S. K.; Wang, S., Chapter 3: Photoresponsive Organoboron Systems. In *Main Group Strategies towards Functional Hybrid Materials*, Baumgartner, T.; Jäkle, F., Eds. 2018; pp 47-77; (q) Pang, S.; Más-Montoya, M.; Manjun Xiao; Duan, C.; Wang, Z.; Liu, X.; Janssen, R.; Yu, G.; Huang, F.; Cao, Y., Adjusting Aggregation Modes, Photophysical and Photovoltaic Properties of Diketopyrrolopyrrole-Based Small Molecules by Introducing B←N Bonds. *Chem.-Eur. J.* **2019**, *25*, 564-572.

8. (a) Wu, J. S.; Pisula, W.; Müllen, K., Graphenes as potential material for electronics. *Chem. Rev.* **2007**, *107*, 718-747; (b) Vadrucci, R.; Weder, C.; Simon, Y. C., Organogels for low-power light upconversion. *Mater. Horiz.* **2015**, *2*, 120-124; (c) Smith, J. N.; Hook, J. M.; Lucas, N. T.,

Superphenylphosphines: Nanographene-Based Ligands That Control Coordination Geometry and Drive Supramolecular Assembly. *J. Am. Chem. Soc.* **2018**, *140*, 1131-1141; (d) Huang, Z. Y.; Tang, M. L., Semiconductor Nanocrystal Light Absorbers for Photon Upconversion. *J. Phys. Chem. Lett.* **2018**, *9*, 6198-6206; (e) Krishnapriya, K. C.; Musser, A. J.; Patil, S., Molecular Design Strategies for Efficient Intramolecular Singlet Exciton Fission. *ACS Energy Lett.* **2019**, *4*, 192−202.

9. (a) Narita, A.; Wang, X. Y.; Feng, X. L.; Müllen, K., New advances in nanographene chemistry. *Chem. Soc. Rev.* **2015**, *44*, 6616-6643; (b) Li, G.; Yoon, K. Y.; Zhong, X. J.; Wang, J. C.; Zhang, R.; Guest, J. R.; Wen, J. G.; Zhu, X. Y.; Dong, G. B., A modular synthetic approach for band-gap engineering of armchair graphene nanoribbons. *Nat. Commun.* **2018**, *9*; (c) Wang, X. Y.; Urgel, J. I.; Barin, G. B.; Eimre, K.; Di Giovannantonio, M.; Milani, A.; Tommasini, M.; Pignedoli, C. A.; Ruffieux, P.; Feng, X. L.; Fasel, R.; Müllen, K.; Narite, A., Bottom-Up Synthesis of Heteroatom-Doped Chiral Graphene Nanoribbons. *J. Am. Chem. Soc.* **2018**, *140*, 9104-9107.

10. Sun, H.; Kabb, C. P.; Dai, Y. Q.; Hill, M. R.; Ghiviriga, I.; Bapat, A. P.; Sumerlin, B. S., Macromolecular metamorphosis via stimulus-induced transformations of polymer architecture. *Nature Chem.* **2017**, *9*, 817-823.

11. (a) Aubry, J. M.; Pierlot, C.; Rigaudy, J.; Schmidt, R., Reversible binding of oxygen to aromatic compounds. *Acc. Chem. Res.* **2003**, *36*, 668-675; (b) Fudickar, W.; Linker, T., Release of Singlet Oxygen from Organic Peroxides under Mild Conditions. *ChemPhotoChem* **2018**, *2*, 548-558; (c) Pibiri, I.; Buscemi, S.; Piccionello, A. P.; Pace, A., Photochemically Produced Singlet Oxygen: Applications and Perspectives. *ChemPhotoChem* **2018**, *2*, 535-547.

12. (a) Martins, S.; Farinha, J. P. S.; Baleizao, C.; Berberan-Santos, M. N., Controlled release of singlet oxygen using diphenylanthracene functionalized polymer nanoparticles. *Chem. Commun.* **2014**, *50*, 3317-3320; (b) Klaper, M.; Linker, T., Intramolecular Transfer of Singlet Oxygen. *J. Am. Chem. Soc.* **2015**, *137*, 13744-13747; (c) Yuan, Z.; Yu, S.; Cao, F. Y.; Mao, Z. W.; Gao, C. Y.; Ling, J., Near-infrared light triggered photothermal and photodynamic therapy with an oxygen-shuttle endoperoxide of anthracene against tumor hypoxia. *Polym. Chem.* **2018**, *9*, 2124-2133.

13. (a) Wu, H. Y.; Song, Q. J.; Ran, G. X.; Lu, X. M.; Xu, B. G., Recent developments in the detection of singlet oxygen with molecular spectroscopic methods. *Trend Analyt. Chem.* **2011**, *30*, 133-141; (b) Altinok, E.; Smith, Z. C.; Thomas, S. W., Two-Dimensional, Acene-Containing Conjugated Polymers That Show Ratiometric Fluorescent Response to Singlet Oxygen. *Macromolecules* **2015**, *48*, 6825-6831.

14. Fudickar, W.; Fery, A.; Linker, T., Reversible light and air-driven lithography by singlet oxygen. *J. Am. Chem. Soc.* **2005**, *127*, 9386-9387.

15. Gao, Z.; Han, Y. F.; Wang, F., Cooperative supramolecular polymers with anthracene. endoperoxide photo-switching for fluorescent anti-counterfeiting. *Nat. Commun.* **2018**, *9*, 3977.

16. (a) Zehm, D.; Fudickar, W.; Linker, T., Molecular switches flipped by oxygen. *Angew. Chem. Int. Ed.* **2007**, *46*, 7689-7692; (b) Zehm, D.; Fudickar, W.; Hans, M.; Schilde, U.; Kelling, A.; Linker, T., 9,10-Diarylanthracenes as Molecular Switches. Syntheses, Properties, Isomerisations and Their Reactions with Singlet Oxygen. *Chem. - Eur. J.* **2008**, *14*, 11429-11441.

17. (a) Mellerup, S. K.; Hafele, L.; Lorbach, A.; Wang, X.; Wang, S. N., Triplet Energy and pi-Conjugation Effects on Photoisomerization of Chiral N,C-Chelate Organoborons with PAH Substituents. *Org. Lett.* **2017**, *19*, 3851-3854; (b) Wang, S. N.; Yuan, K.; Hu, M. F.; Wang, X.; Peng, T.; Wang, N.; Li, Q. S., Cleavage of Unstrained C-C Bonds in Acenes by Boron and Light: Transformation of Naphthalene into Benzoborepin. *Angew. Chem. Int. Ed.* **2018**, *57*, 1073-1077.

18. (a) Pais, V. F.; Lineros, M.; Lopez-Rodriguez, R.; El-Sheshtawy, H. S.; Fernandez, R.; Lassaletta, J. M.; Ros, A.; Pischel, U., Preparation and pH-Switching of Fluorescent Borylated Arylisoquinolines for Multilevel Molecular Logic. *J. Org. Chem.* **2013**, *78*, 7949-7961; (b) Pais, V. F.; El-Sheshtawy, H. S.; Fernandez, R.; Lassaletta, J. M.; Ros, A.; Pischel, U., Borylated Arylisoquinolines: Photophysical Properties and Switching Behavior of Promising Tunable Fluorophores. *Chem-Eur J* **2013**, *19*, 6650-6661; (c) Pais, V. F.; Lassaletta, J. M.; Fernandez, R.; El-Sheshtawy, H. S.; Ros, A.; Pischel, U., Organic Fluorescent Thermometers Based on Borylated Arylisoquinoline Dyes. *Chem.-Eur. J.* **2014**, *20*, 7638-7645; (d) Bosca, F.; Cuquerella, M. C.; Pais, V. F.; Ros, A.; Pischel, U., Excited-State Pathways of Four-Coordinate N,C-Chelate Organoboron Dyes. *ChemPhotoChem* **2018**, *2*, 34-41.

19. (a) Shen, C. S.; Srebro-Hooper, M.; Jean, M.; Vanthuyne, N.; Toupet, L.; Williams, J. A. G.; Torres, A. R.; Riives, A. J.; Muller, G.; Autschbach, J.; Crassous, J., Synthesis and Chiroptical Properties of Hexa-, Octa-, and Deca-azaborahelicenes: Influence of Helicene Size and of the Number of Boron Atoms. *Chem.-Eur. J.* **2017**, *23*, 407-418; (b) Dominguez, Z.; Lopez-Rodriguez, R.; Alvarez, E.; Abbate, S.; Longhi, G.; Pischel, U.; Ros, A., Azabora[5]helicene Charge-Transfer Dyes Show Efficient and Spectrally Variable Circularly Polarized Luminescence. *Chem.-Eur. J.* **2018**, *24*, 12660-12668.

20. Stolar, M.; Baumgartner, T., Functional conjugated pyridines via main-group element tuning. *Chem. Commun.* **2018**, *54*, 3311-3322.

21. (a) 9- or 9,10-borylated anthracenes are more common; see: ; (b) Yamaguchi, S.; Akiyama, S.; Tamao, K., Tri-9-anthrylborane and its Derivatives: New Boron-Containing p-Electron Systems with Divergently Extended p-Conjugation through Boron. *J. Am. Chem. Soc.* **2000**, *122*, 6335-6336; (c) Uchida, M.; Ono, Y.; Yokoi, H.; Nakano, T.; Furukawa, K., Undoping Type of Highly Efficient Organic Light Emitting Diodes. *J. Photopolym. Sci. Technol.* **2001**, *14*, 305-310.

22. Liu, K. L.; Lalancette, R. A.; Jäkle, F., B-N Lewis Pair Functionalization of Anthracene: Structural Dynamics, Optoelectronic Properties, and O2 Sensitization. *J. Am. Chem. Soc.* **2017**, *139*, 18170-18173.

23. Yang, C.; Jacob, J.; Müllen, K., Synthesis and photochromic properties of ladderized poly(p-phenylene-alt-9,10-anthrylene)s. *Macromolecules* **2006**, *39*, 5696-5704.

24. Ingleson, M. J., A perspective on direct electrophilic arene borylation. *Synlett* **2012**, *23*, 1411-1415.

25. Fudickar, W.; Linker, T., Synthesis of Pyridylanthracenes and Their Reversible Reaction with Singlet Oxygen to Endoperoxides. *J. Org. Chem.* **2017**, *82*, 9258-9262.

26. (a) Schaffner, K.; Schmidt, R.; Brauer, H.-D., Photochromism based on the reversible reaction of singlet oxygen with aromatic compounds. *Mol. Cryst. Liq. Cryst.* **1994**, *246*, 119-125; (b) Seip, M.; Brauer, H. D., Endoperoxide Formation of Helianthrene with Triplet Molecular-Oxygen - a Spin-Forbidden Reaction. *J. Am. Chem. Soc.* **1992**, *114*, 4486-4490.

27. (a) Fudickar, W.; Linker, T., Remote substituent effects on the photooxygenation of 9,10-diarylanthracenes: strong evidence for polar intermediates. *Chem. Commun.* **2008**, 1771-1773; (b) Fudickar, W.; Linker, T., Why Triple Bonds Protect Acenes from Oxidation and Decomposition. *J. Am. Chem. Soc.* **2012**, *134*, 15071-15082.

28. Fudickar, W.; Linker, T., Release of Singlet Oxygen from Aromatic Endoperoxides by Chemical Triggers. *Angew. Chem. Int. Ed.* **2018**, *57*, 12971-12975.

TOC Entry

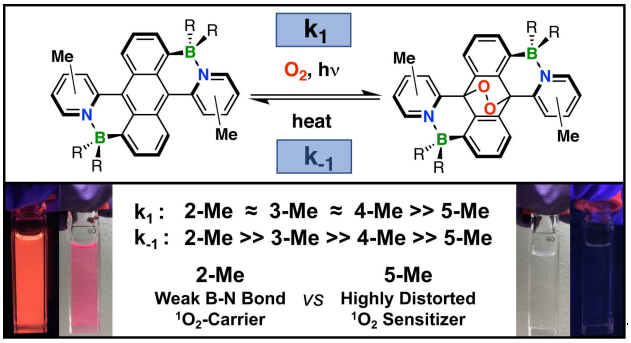
k1
O2, hν
heat
k-1
Me
Me
Me
Me
R
R
B
N
O
O
k1 : 2-Me ≈ 3-Me ≈ 4-Me >> 5-Me
k-1 : 2-Me >> 3-Me >> 4-Me >> 5-Me
2-Me
Weak B-N Bond
1O2-Carrier
vs
5-Me
Highly Distorted
1O2 Sensitizer